The Harmony of Gravity, Turbulence, and Magnetic Field in the Formation of the Prestellar Core, L1544

Shinyoung Kim[1], Chang Won Lee[1,2], Mario Tafalla[3], Philip C. Myers[4], Maheswar Gophinathan[5], Paola Caselli[6], Eun Jung Chung[7], and the **JCMT BISTRO** Survey members

e-mail: *shinykim@kasi.re.kr* / [1]KASI-Korea, [2]UST-Korea, [3]OAN(IGN)-Spain, [4]CfA-USA, [5]IIA-India, [6]MPE(MPI)-Germany, [7]CNU-Korea

I. Introduction and Observations

- **Detailed processes of dense core formation are crucial in star formation**
  - ‣ Quasi-static contraction via ambipolar diffusion (e.g., Mouschovias 1991)
  - ‣ Turbulence dissipation by collisions of supersonic flows (e.g., Klessen et al. 2005)
  - ‣ Filament fragmentation by gravitational instability (e.g., Inutsuka & Miyama 1997)

- **Prestellar cores are formed in filamentary structure**
  - ‣ Molecular clouds consist of filamentary structures (e.g., André et al. 2010)
  - ‣ Prestellar cores are in locations related to filaments (e.g., Könyves et al. 2015)

How Do Dense Cores Form in Their Natal Filament?

- **What is the role of filaments in core formation?**
- **Which of gravity, turbulence, or magnetic fields drives this process?**

Prestellar Core, L1544 in Taurus

- **Highly evolved, gravitationally unstable, and infall motions** (e.g., Lee et al. 2001)
- **Embedded in isolated, pc-scale filamentary clouds**
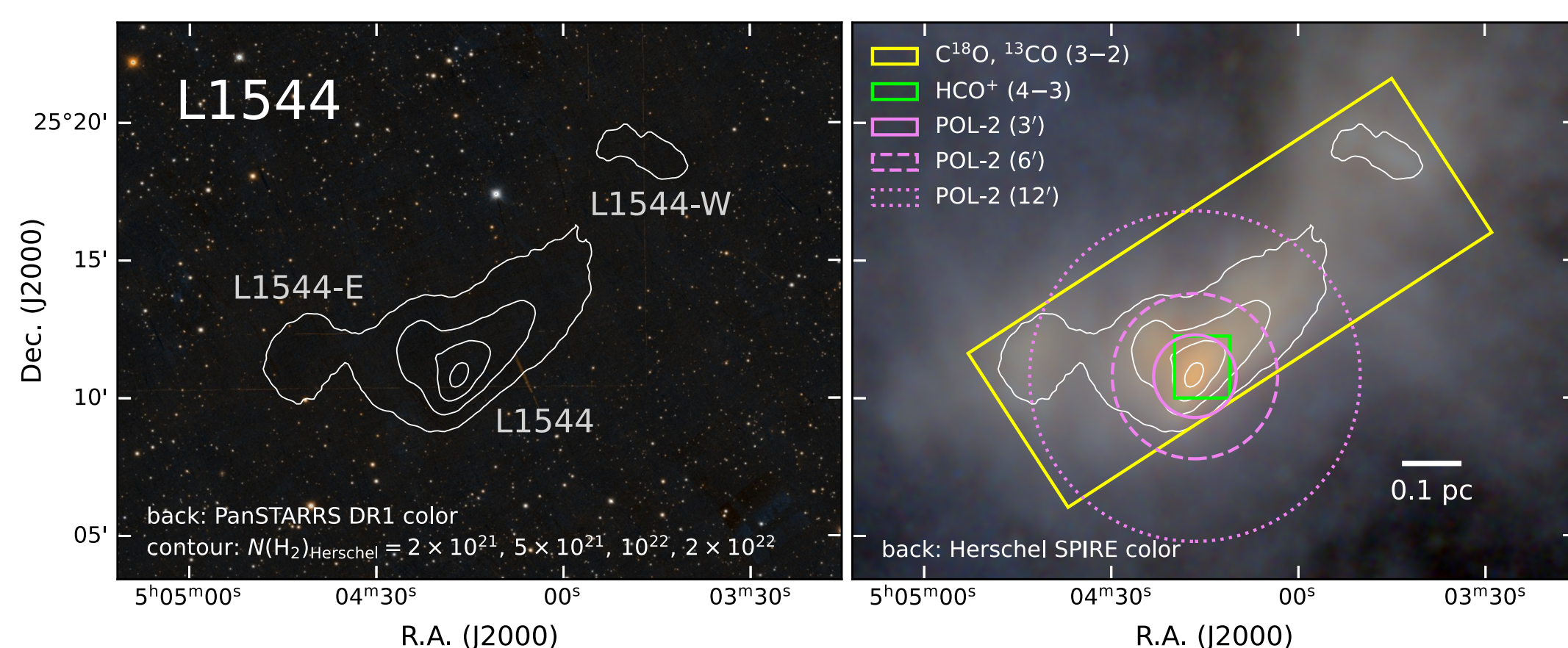

Fig. 1. L1544 shown in optical (left, Pan-STARRS DR 1 color) and far-IR (right, Herschel SPIRE color) images (left panel). The mapping areas with molecular lines and dust polarization using JCMT/HARP and JCMT/SCUBA-2/POL-2, respectively (right panel).

Molecular Lines
(Kim et al. 2022, ApJ, 940, 112)

- **JCMT / HARP mapping**
  - ‣ PID: M16AP025, M17AP061
  - ‣ ^{13}CO, C^{18}O (3–2), HCO$^+$ (4–3)
  - ‣ HPBW~14″, δV~0.03–0.06 km s^{-1}
- **Complemented by Herschel PACS / SPIRE dust continuum data**

Dust Polarization
(Kim et al. 2023, in preparation)

- **JCMT / SCUBA-2 / POL-2**
  - ‣ **JCMT BISTRO Survey**
    (PI: Derek Ward-Thompson)
  - ‣ M20AL018
  - ‣ 850 (and 450) μm continuum
  - ‣ effective FWHM~14″.6

II. Density Structures

Filamentary Structure of L1544

- **0.5 pc-long main filament and 0.2 pc-long branch**
  - ‣ M_{fil}~7 M$_\odot$ (main), 3 M$_\odot$ (branch), M_{line}~16 M$_\odot$
  - ‣ similar to the velocity-coherent fibers
    (Hacar et al. 2013)

New Distance!
D ~ 175 pc

Gaia DR2 parallax + Pan-STARRS catalog

Fig. 2. Determination of L1544 distance. The red line indicates the best-fit distance, and the blue dashed lines show the extinction of foreground and background stars.
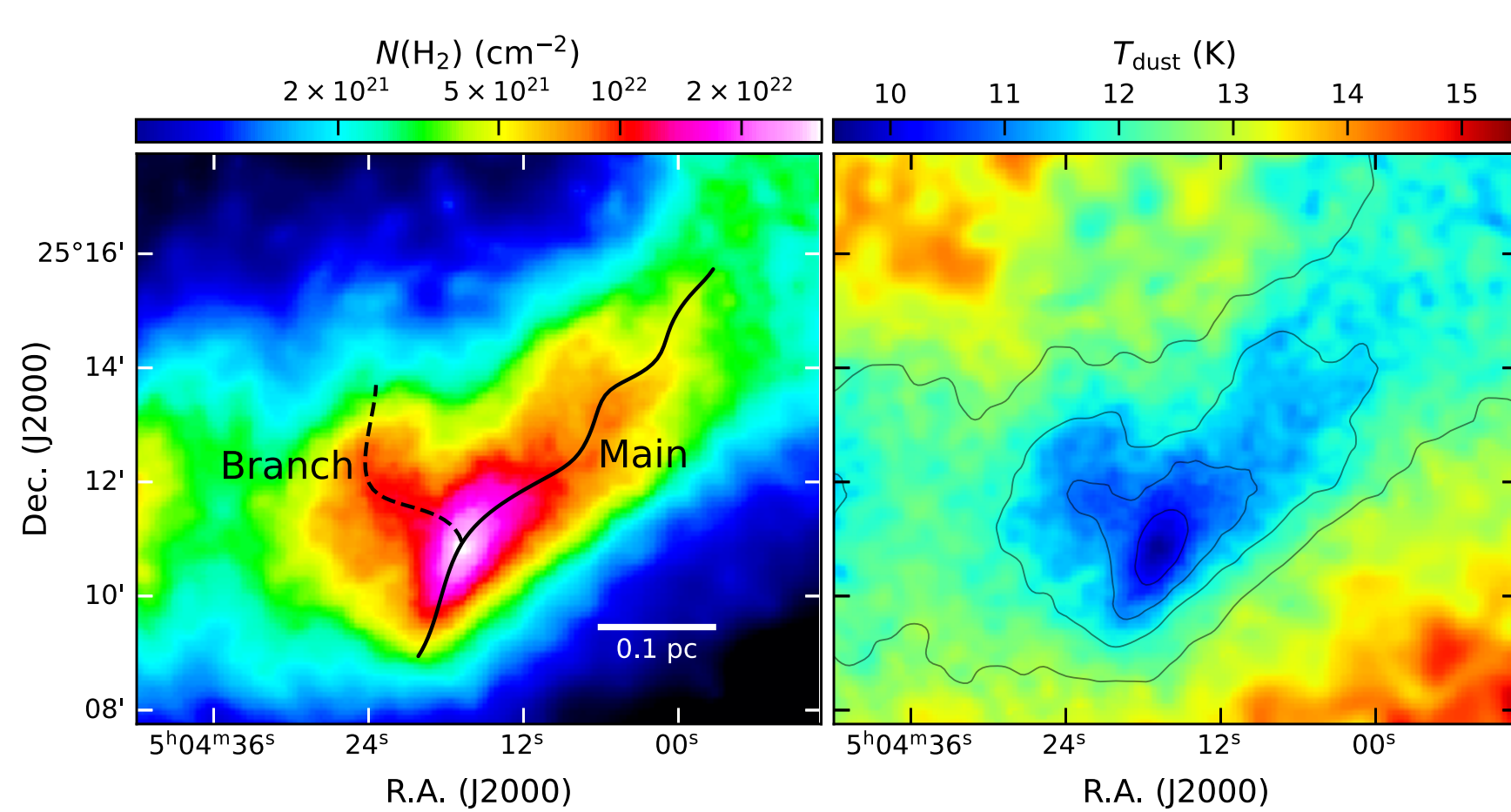

Fig. 3. Distribution of H$_2$ column density (left) and dust temperature (right) in L1544 derived from the SED fit for Herschel dust continuum data. The black solid and dashed lines on the left panel show the skeleton of the filamentary structure identified using the **FilFinder** algorithm (Koch & Rosolowsky 2015).

V. Formation of L1544

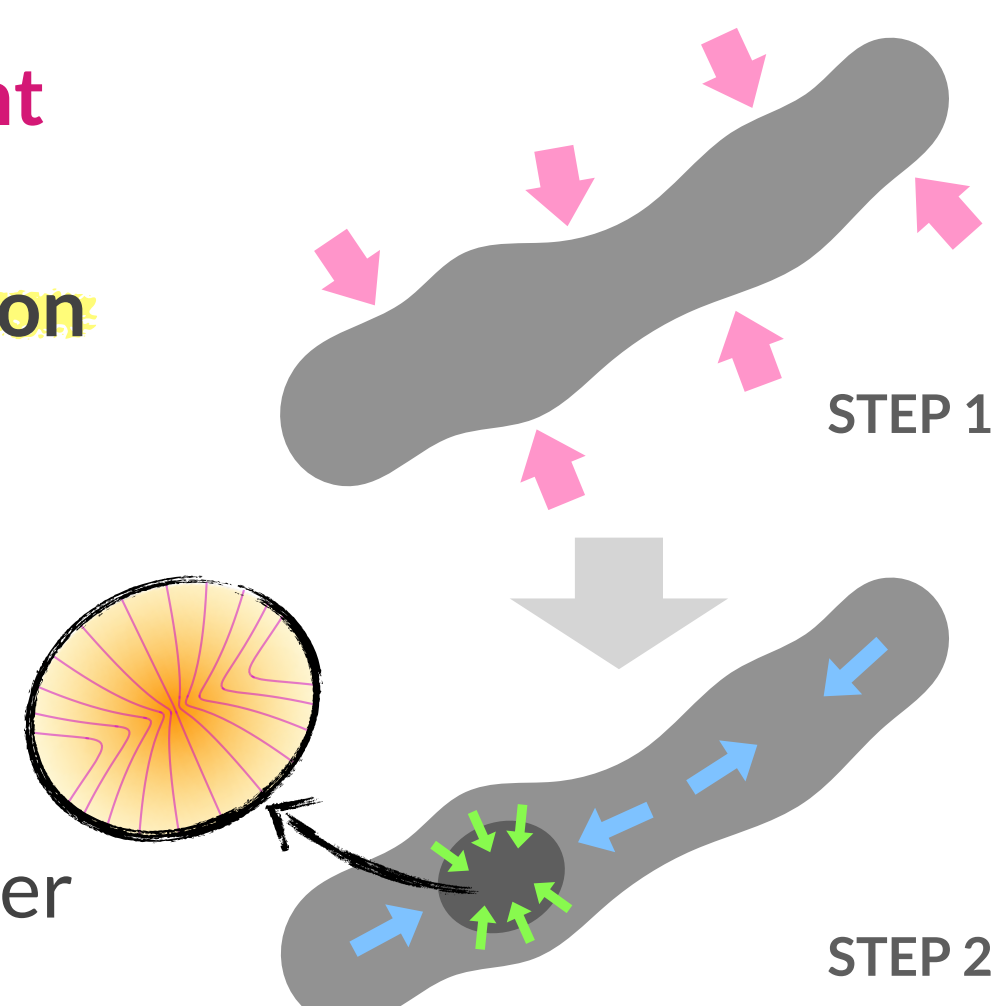**Step 1. Formation of velocity-coherent filament**
- ‣ collision of large-scale turbulence flow
- ‣ filament formation by turbulence dissipation

Step 2. Filament fragmentation into core(s)
- ‣ shock-induced? or gravitational instability?

- **Magnetic field supports core contraction**
  - ‣ structure aligned to B-field
  - ‣ hourglass-shaped field in infalling core center

III. Velocity Structures

- **Velocity centroid and dispersion** ← Gaussian fit for C^{18}O and ^{13}CO (3–2) line profiles
- **Large-scale velocity difference across the filament: ΔV~0.6 km s^{-1}**
  - ‣ implying the presence of large-scale turbulence flows and their collision

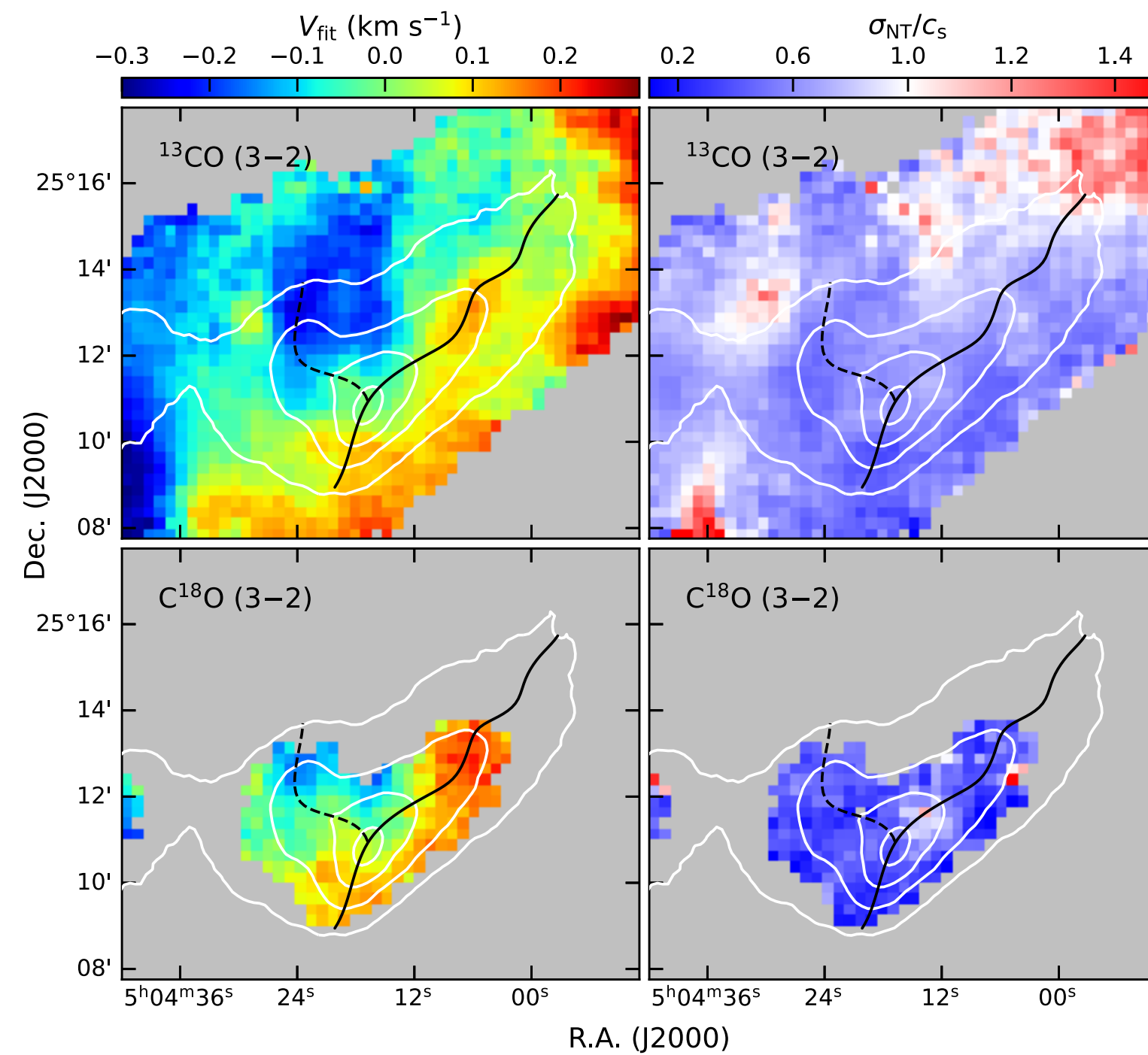Fig. 4. Distribution of velocity centroid (V_{fit}) and non-thermal dispersion (σ_{NT}) measured with Gaussian fit for C^{18}O and ^{13}CO (3–2) line profiles. The V_{fit} is displayed by the velocity difference from 7.12 km s^{-1}, and the σ_{NT} is expressed in the sonic Mach number.

Velocity-Coherent and Subsonic

- **Velocity along filament axis continuously changes w/o large dispersion**
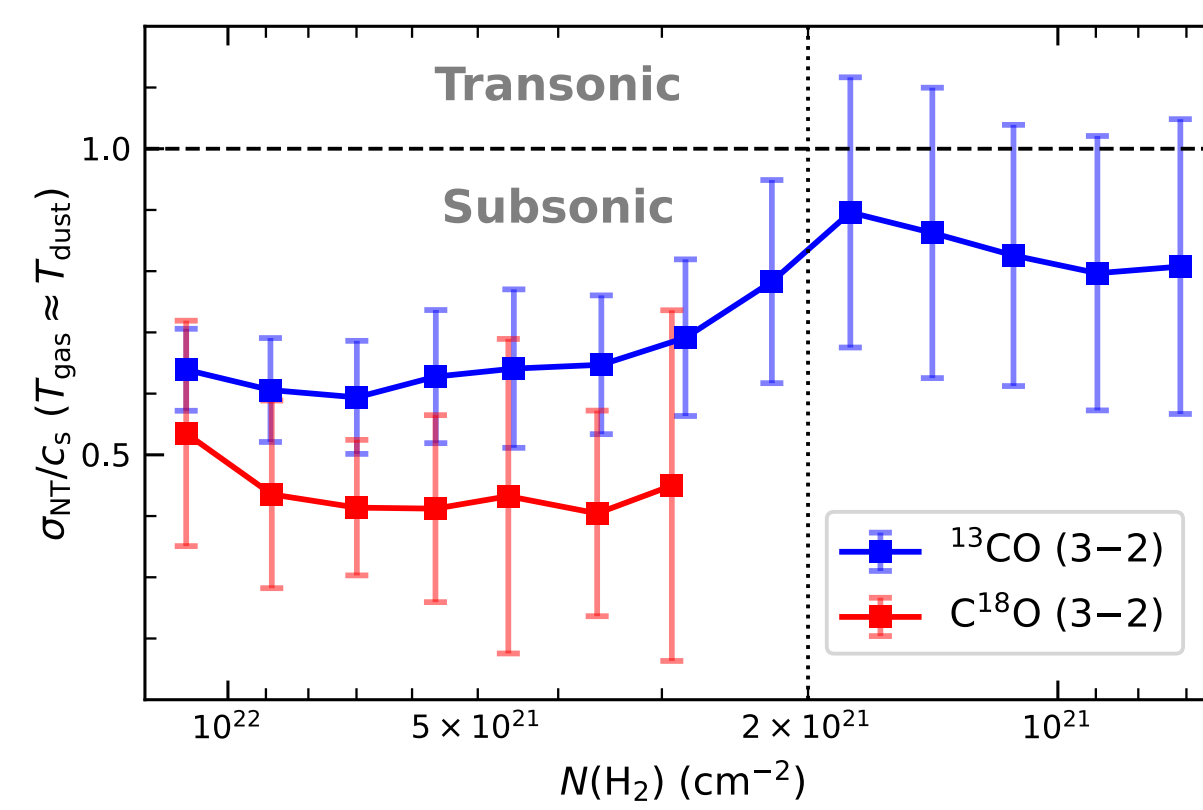- **Core and filament are mostly subsonic**

Fig 6. Variation of non-thermal velocity dispersion with respect to the H$_2$ column density. The dotted vertical line indicates the filament boundary.

Core-Forming Flow Motion Along the Filament Axis

- **Linear velocity gradient across the core**
  - ‣ ∇V_l~1.5 km s^{-1} pc^{-1}, $\dot{M}_l$~3 M$_\odot$ Myr^{-1}
- **Longitudinal filament fragmentation**
  - ‣ **λ/4 shift between velocity and density variation** (e.g., Hacar & Tafalla 2011)
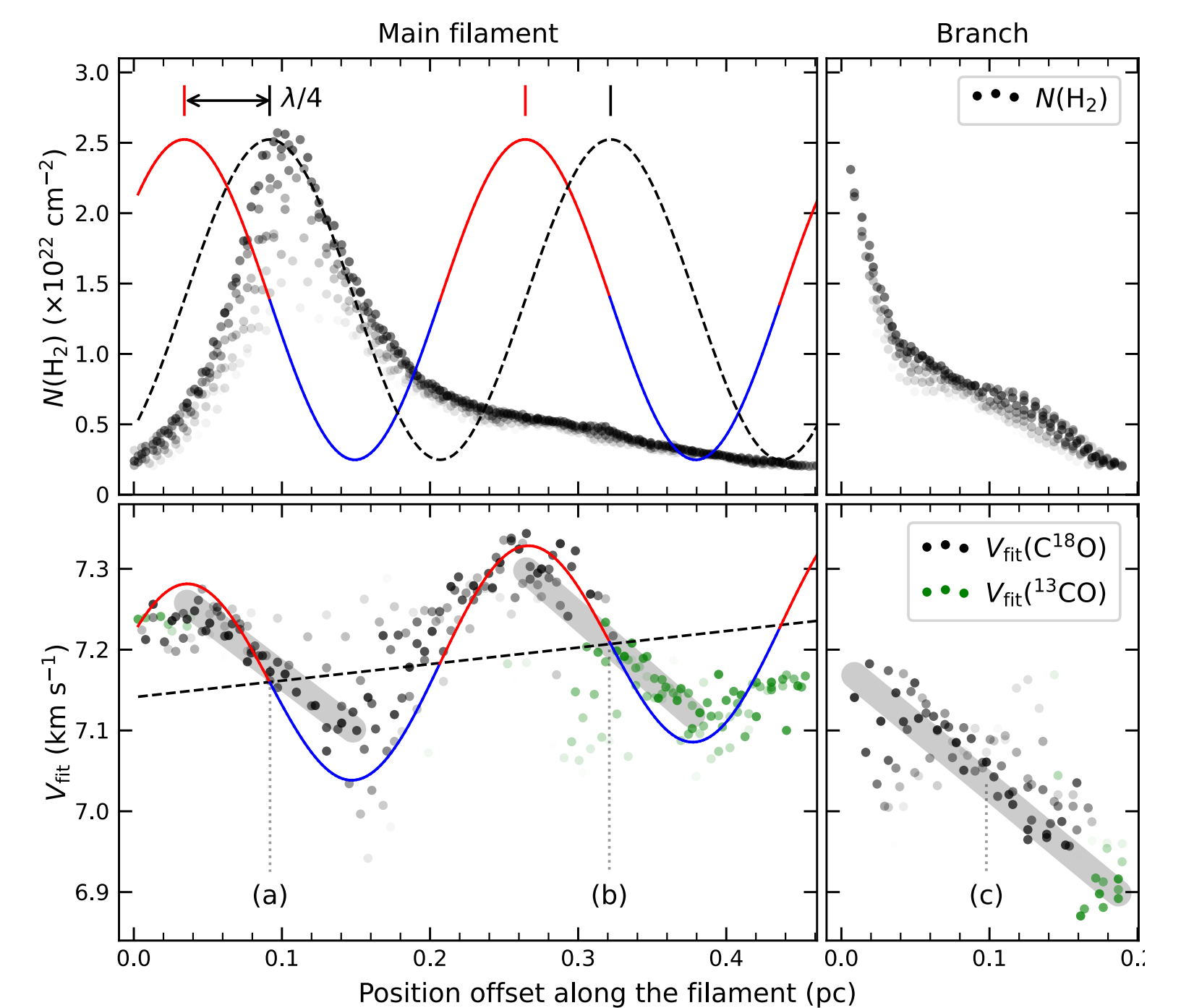

Fig. 5. Axial variation of N(H$_2$) and V_{fit} along the filament. *In lower panels:* The red and blue curve is the best-fit model of sinusoidal velocity oscillation. The thick grey lines are to show the local velocity gradients. *In upper panels:* The red and blue sinusoidal curve is expressed with the same wavelength and phase of the best-fit model, and the black dashed curve is a λ/4 shifted one.

IV. B-field Structures

- **B-field in the prestellar core with magnetic support**
  - ‣ **Expectation: hourglass-shaped θ_B, ⟨θ_B⟩ ⊥ major-axis of core (or main-axis of filament)**
  - ‣ Observation (*before POL-2*): ordered and linear, ~20° offset ⟨θ_B⟩ and minor-axis of core

Hourglass-shaped B-field of Prestellar Core in sub-mm

- **First detection of hourglass-shaped B-field morphology**
  - ‣ B-vectors follow the field line pinched completely toward the core center.

- **Highly consistent with the 'Spheroid Flux Freezing (SFF)' model** (Myers et al. 2018, 2020)
  - ‣ Plummer-like spheroid density (perpendicular prolate) + SFF B-field direction
    - Except for inclination angle, all other parameters were optimized based on N(H$_2$) map
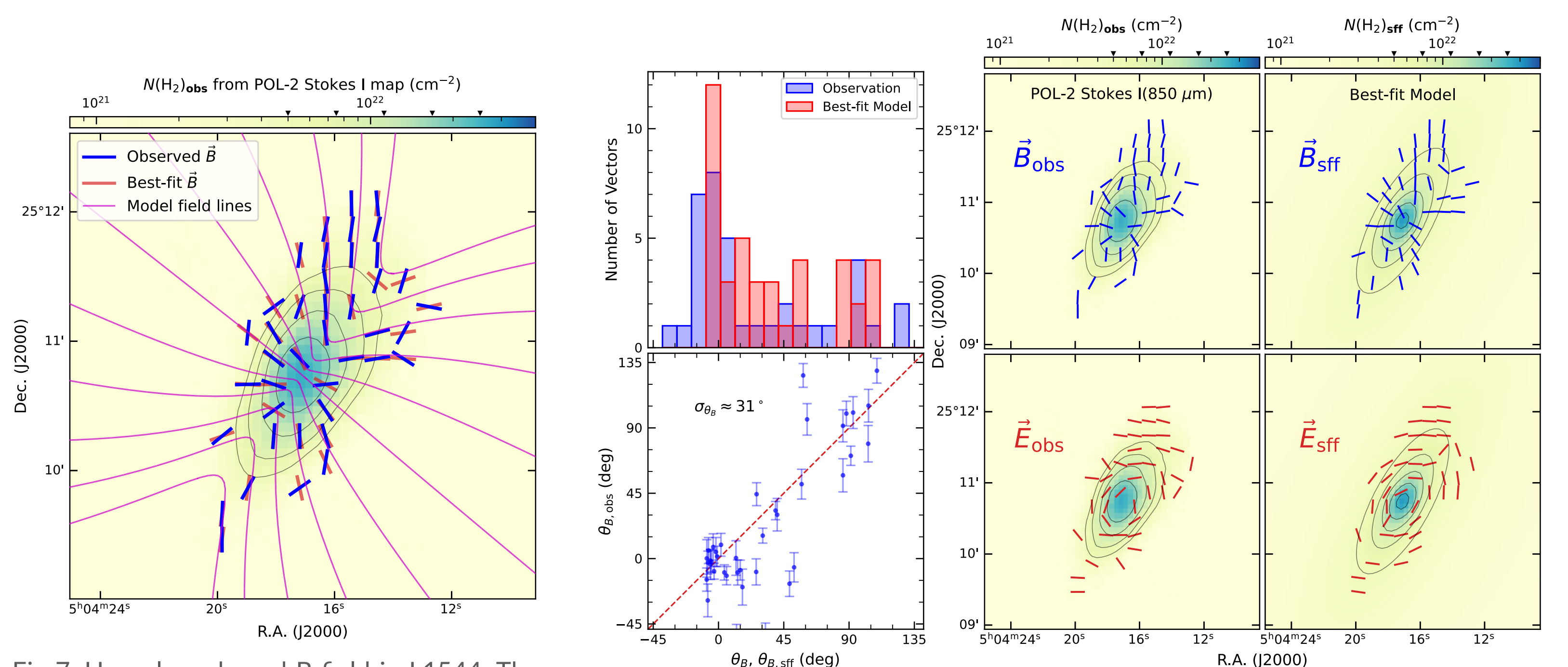 - ‣ **Mean field direction and minor axis of the spheroid are well aligned.**

Fig 7. Hourglass-shaped B-field in L1544. The vectors in blue are from POL-2 observation, and The red ones show the field direction of the best-fit SFF model on each detected pixel. The violet curves show the plane-of-sky field lines at the core center.

Fig 8. Comparison of the observed polarization vector (rotated to 90°) and the B-field directions of the best-fit SFF model. In center panels, the background N(H$_2$) map and the polarization vectors were derived from POL-2 850 μm Stokes I, Q, and U maps. The column densities and field vectors of the best-fit model were displayed in right panels.